THE JOURNAL OF PHYSICAL CHEMISTRY C

Article

pubs.acs.org/JPCC

Structural and Luminescence Properties of Yellow-Emitting $NaScSi_2O_6$:Eu^{2+} Phosphors: Eu^{2+} Site Preference Analysis and Generation of Red Emission by Codoping Mn^{2+} for White-Light-Emitting Diode Applications

Zhiguo Xia,*[,†] Yuanyuan Zhang,[†] Maxim S. Molokeev,[‡] and Victor V. Atuchin[§]

[†]School of Materials Sciences and Technology, China University of Geosciences, Beijing 100083, China

[‡]Laboratory of Crystal Physics, Kirensky Institute of Physics, SB RAS, Krasnoyarsk 660036, Russia

[§]Laboratory of Optical Materials and Structures, Institute of Semiconductor Physics, SB RAS, Novosibirsk 630090, Russia

Supporting Information

ABSTRACT: The structural properties of clinopyroxene $NaScSi_2O_6$ have been investigated using the X-ray powder diffraction refinement, and the luminescence properties of Eu^{2+} and Eu^{2+}/Mn^{2+}-activated $NaScSi_2O_6$ have been studied to explore the new materials for phosphor-converted white light ultraviolet light-emitting diodes (UV-LEDs). Eu^{2+} was introduced into the $NaScSi_2O_6$ host in the reducing atmosphere, and the preferred crystallographic positions of the Eu^{2+} ions were determined based on the different structural models of the $NaScSi_2O_6$ host. The as-obtained $NaScSi_2O_6$:Eu^{2+} phosphor shows greenish yellow emission with the broad-band peak at 533 nm, and efficient energy transfer (ET) takes place between Eu^{2+} and Mn^{2+} in $NaScSi_2O_6$, leading to a series of color-tunable phosphors emitting at 533 and 654 nm for the designed $NaScSi_2O_6$:Eu^{2+},Mn^{2+} phosphors under excitation at 365 nm. The ET mechanism of Eu^{2+} and Mn^{2+} has also been evaluated. We have demonstrated that $NaScSi_2O_6$:Eu^{2+} and $NaScSi_2O_6$:Eu^{2+},Mn^{2+} materials exhibit great potential to act as the effective phosphors for UV-LEDs.

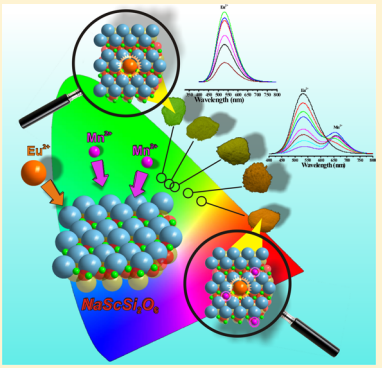

1. INTRODUCTION

White-light-emitting diodes (*w*-LEDs) lighting technology has attracted significant attention, and there is an increasing interest for white light based *w*-LEDs as a potential replacement for the incandescent and fluorescent light sources.[1,2] The present industrial method to produce the white light is to combine blue LEDs with yellow emission from the $Y_3Al_5O_{12}$:Ce^{3+} (YAG:Ce) phosphors. However, the low color-rendering index (R_a) and high correlated color temperature (CCT) due to the deficiency of red emission in the visible spectrum restrict some primary applications.[3−5] Recently, the *w*-LEDs fabricated using near-ultraviolet (*n*-UV) light (350−420 nm) chips coupled with the multicolor-emitting phosphors have been widely reported to exhibit favorable properties.[6−8] Among them, the development of new yellow-emitting phosphors becomes a hot issue. Accordingly, many new yellow phosphors for the *n*-UV *w*-LEDs have been reported, such as $Sr_8ZnSc(PO_4)_7$:Eu^{2+},[9] $Ba_2Gd(BO_3)_2Cl$:Eu^{2+},[10] $Y_2(CN_2)_3$:Ce^{3+},[11] $Na_3K(Si_{1-x}Al_x)_8O_{16}$:$Eu^{2+}$,[12] and so on. In this study, we explore the novel phosphor, $NaScSi_2O_6$:Eu^{2+}, which emits greenish yellow luminescence upon violet excitation with as high internal quantum efficiency as 71.7% (λ_{ex} = 365 nm). To further overcome the deficiency of the red component, the red-emitting Mn^{2+} ions were codoped into the $NaScSi_2O_6$:Eu^{2+} phosphors. As expected, a series of emission tunable phosphors from greenish yellow to orange emission colors were obtained by adjusting the Eu^{2+}/Mn^{2+} ratio. To the best of our knowledge, the yellow-emitting $NaScSi_2O_6$:Eu^{2+} phosphor, as well as the energy transfer mechanism and color-tunable emission of $NaScSi_2O_6$:Eu^{2+}, Mn^{2+} phosphor, have not been reported up to now.

As for the studied clinopyroxene $NaScSi_2O_6$ host, the compound belongs to the Na-clinopyroxene family with general composition of $NaMe^{3+}Si_2O_6$ with Me^{3+} in the octahedral coordination and monoclinic structure in space group *C*2/*c* at ambient conditions.[13,14] The Na-clinopyroxene silicates are known to be stable over a wide range of pressures and temperatures and are widely investigated as the functional materials for different applications owing to the variable crystal chemistry tolerance. As for phosphor hosts, it is well-known that the doping ion sites and the crystal field environment around activators have a very important influence on the luminescence properties.[15,16] In the $NaScSi_2O_6$ host, however, it is hard to predict whether Eu^{2+} ions enter the Na^+ or Sc^{3+} sites owing to the different charge characteristics, regardless of the observed excellent optical properties of the phosphor.

Received: June 24, 2013
Revised: July 31, 2013
Published: August 2, 2013

   dx.doi.org/10.1021/jp4062225 | *J. Phys. Chem. C* 2013, 117, 20847−20854

Therefore, except for the exploration of the photoluminescence behavior, one of the main tasks of the present study is to investigate the structural properties of doped $NaScSi_2O_6$ by the X-ray powder diffraction methods. As a result, the preferred crystallographic positions of the Eu^{2+} ions were determined through the comparison of different structural models tested for doped $NaScSi_2O_6$. Therefore, the relationship between the structure and luminescence properties is considered in this investigation. Furthermore, we have also successfully fabricated the *n*-UV *w*-LED lamp using the yellow-orange-emitting $NaScSi_2O_6:Eu^{2+},Mn^{2+}$ samples and the commercial blue-emitting $BaMgAl_{10}O_{17}:Eu^{2+}$ ($BAM:Eu^{2+}$) phosphors in combination with the 370 nm *n*-UV LED chip, and optical properties of the device have been examined. The results indicate that the reported phosphors have a great potential for applications in the *n*-UV *w*-LEDs lamps.

2. EXPERIMENTAL SECTION

2.1. Sample Preparation. All the Eu^{2+} and Eu^{2+}/Mn^{2+} doped $NaScSi_2O_6$ phosphors were prepared using the sol−gel method.[17−21] The starting materials of Eu_2O_3 (>99.99%) and $Sc(NO_3)_3$ were supplied by China Minls (Beijing) Research Institute, Beijing, China, and $MnCO_3$ (>99.5%), $NaNO_3$ (>99.5%), and $Si(OC_2H_5)_4$ (>99.5%) were purchased from Sinopharm Chemical Reagent Co. Ltd., Shanghai, China. In a typical process of the preparation of $NaScSi_2O_6:Eu^{2+}/Mn^{2+}$ phosphor, Eu_2O_3 and $MnCO_3$ were dissolved in HNO_3 to obtain soluble $Eu(NO_3)_3$ and $Mn(NO_3)_2$ powders. Then the stoichiometric amounts of $NaNO_3$ and $Sc(NO_3)_3$ were dissolved in ethanol under stirring. After this, the designed amounts of $Eu(NO_3)_3$, $Mn(NO_3)_2$, and $Si(OC_2H_5)_4$ were added successively in the solution. The resultant mixtures were stirred at 80 °C for 30 min until the formation of homogeneous gels. After drying at 120 °C for 12 h in an oven, the gels were ground and preferred at 800 °C for 20 h in the air and then fully ground and sintered at 1200 °C in the CO reducing atmosphere for 5 h. After that, the samples were furnace-cooled to room temperature and ground again into fine powders. Thus, the Eu^{2+} and Eu^{2+}/Mn^{2+} doped $NaScSi_2O_6$ phosphors were finally obtained for the following investigation.

2.2. Sample Characterization. Powder X-ray diffraction data were collected by a Panalytical X'pert diffractometer with Cu Kα radiation at 40 kV and 40 mA. The data for Rietveld analysis were collected in a step mode with the step size of 0.02° and 20 s counting time per step over the 2θ range from 10° to 135°, and the X-ray beam was controlled by a 0.5° fixed divergence slit. Diffuse reflection spectra of the as-synthesized phosphors were measured using a UV−vis−NIR spectrophotometer (SHIMADZU UV-3600) attached with an integrating sphere. The $BaSO_4$ sample was used as a reference standard. Room-temperature photoluminescence excitation (PLE) and emission (PL) spectra were characterized by a F-4600 fluorescence spectrophotometer with the photomultiplier tube operating at 400 V and the 150 W Xe lamp used as the excitation source. The decay curves were recorded by a spectrofluorometer (HORIBA, JOBIN YVON FL3-21) where the 370 nm pulse laser radiation (nano-LED) was used as the excitation source. The quantum efficiency (QE) was measured by an Absolute Photoluminescence Quantum Yield Measurement System (C9920-02, Hamamatsu-Photonics) with an integrating sphere at room temperature.

2.3. *w*-LED Lamp Fabrication. The white-light *n*-UV LED was fabricated using a mixture of silicon resin, the as-prepared yellow-orange-emitting $NaScSi_2O_6:Eu^{2+},Mn^{2+}$ phosphor, and commercial blue-emitting $BaMgAl_{10}O_{17}:Eu^{2+}$ phosphor, which were dropped onto a 370 nm UV chip. The optical properties, including the luminescent spectrum, R_a, CCT, and CIE value of the lamp, were measured by a HAAS-2000 (Everfine, China) light and radiation measuring instrument.

3. RESULTS AND DISCUSSION

3.1. Eu^{2+} Site Preference Analysis. X-ray patterns of the title compound with the nominal composition of $Na_{0.9}Eu_{0.1}ScSi_2O_6$ were successfully indexed in the monoclinic *C*2/*c* space group with unit cell parameters of a = 9.831 Å, b = 9.068 Å, c = 5.341 Å, and β = 107.01° (Gof = 10.6) using the program TOPAS 4.2.[22] Almost all peaks were indexed except several small impurity peaks. It was concluded that the $Na_{0.9}Eu_{0.1}ScSi_2O_6$ solution is iso-structural to $NaScSi_2O_6$, clinopyroxene.[13,14] It is known that pure $NaScSi_2O_6$ crystallizes in monoclinic space group *C*2/*c*, but there are two points of view in the reported references on the crystal structure leading to two cation models: (i) $(Na_{0.5}Sc_{0.5})(Sc_{0.5}Na_{0.5})Si_2O_6$, where the (0, 0.3036, 1/4) position is occupied by half Na and half Sc and the (0, 0.8961, 1/4) position by half Sc and half Na also;[13] (ii) $NaScSi_2O_6$, where the (0, 0.3036, 1/4) position is occupied by Na and the (0, 0.8961, 1/4) position by Sc.[14] So, we have tried to refine the structure of $Na_{0.9}Eu_{0.1}ScSi_2O_6$ in both the models. Eu^{2+} was placed in all the (0, 0.3036, 1/4) and (0, 0.8961, 1/4) positions, and occupancies were refined. The sum of occupancies of all atoms in each position was taken to be equal to 1. The refinements have been performed by program TOPAS 4.2, and the Rietveld analysis patterns of $Na_{0.9}Eu_{0.1}ScSi_2O_6$ fulfilled in model (i) and model (ii) are shown in Figures 1a and 1b, respectively. The main parameters of processing and refinement are reported in Table 1.

One can see that model (i) is not acceptable for the $Na_{0.9}Eu_{0.1}ScSi_2O_6$ solution because of high *R*-factors and unusual thermal parameters given in Table S1 in the Supporting Information. On the contrary, model (ii) gives a good result, as is shown in Table 1, Table S1 (Supporting Information), and Figure 1b. Moreover, model (i) has internal contradiction since the effective ion radius $R(Na^+_{CN=6})$ = 1.02 Å is too big to penetrate the Na^+ ion into the (0, 0.8961, 1/4) position occupied by Sc^{3+} with $R(Sc^{3+}_{CN=6})$ = 0.745 Å without structure deformation.[23] Therefore, we concluded that model (ii) should be valid. From the observation of the model (ii) parameters shown in Table S1 (Supporting Information), one can see that the Eu partial occupancy in the Sc site is equal to 0. Only in the Na position the nonzero value of the Eu occupancy is found. This result can be supposed from general information on the effective ion radii in oxides because the Sc site is very small for the Eu^{2+} ion.

The crystal structure of as-prepared $Na_{0.9}Eu_{0.1}ScSi_2O_6$ depicted in model (ii) is presented in Figure 2a, and the structure does not show strong deviation from iso-structural $NaScSi_2O_6$.[14] The detailed information on the crystal structure of $Na_{0.9}Eu_{0.1}ScSi_2O_6$ can be found in the CIF file in the Supporting Information. The bond distances and angles are found to be within the conventional ranges for all atoms as shown in Table S2 (Supporting Information). To illustrate the evidence of the Eu^{2+} preferred sites, the schematic diagram of the dimensional relationship of the Na^+, Sc^{3+}, and doped Eu^{2+} ions in the $NaScSi_2O_6$ host is depicted in Figure 2b. The effective ion radii (IR) of $Sc^{3+}_{CN=6}$ = 0.745 Å, IR of $Na^+_{CN=8}$ = 1.18 Å, and IR of $Eu^{2+}_{CN=6-8}$ = 1.17−1.25 Å in oxides are well-

dx.doi.org/10.1021/jp4062225 | J. Phys. Chem. C 2013, 117, 20847−20854

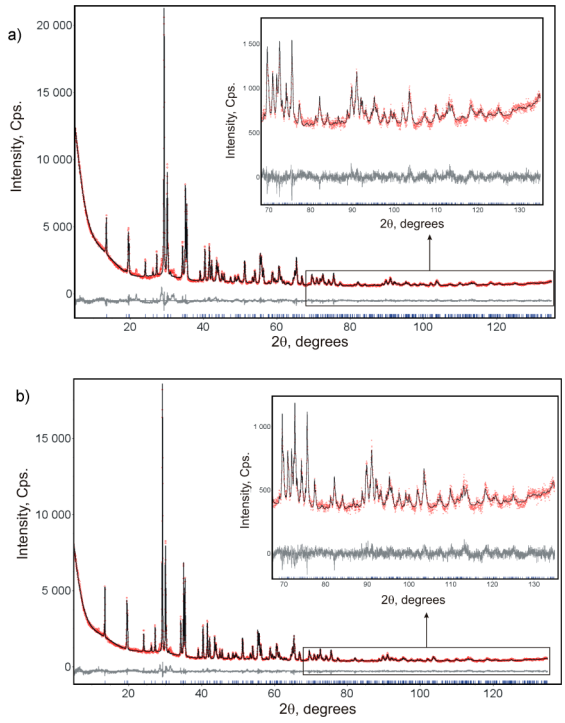

Figure 1. Rietveld difference plots of as-prepared $Na_{0.9}Eu_{0.1}ScSi_2O_6$ samples based on (a) model (i) and (b) model (ii). Some disagreements at low 2θ in difference plot of model (i) are demonstrated.

Table 1. Main Parameters of Processing and Refinement of the $Na_{0.9}Eu_{0.1}ScSi_2O_6$ Sample

parameters	model (i)	model (ii)
Sp. Gr.	*C*2/*c*	
a_i, Å	9.8339(4)	9.8336(4)
b_i, Å	9.0740(4)	9.0741(3)
c_i, Å	5.3447(2)	5.3446(2)
β, °	107.022(2)	107.021(2)
V, Å^3	456.03(3)	456.01(3)
Z	1	
2θ-interval, °	5−135	
number of reflections	416	
number of parameters of refinement	75	
R_{wp}, %	6.307	5.864
R_p, %	4.272	3.961
R_{exp}, %	2.665	2.665
χ	2.366	2.200
R_B, %	2.507	1.923
thermal parameters of atoms	unusual	acceptable

known. Evidently, the Sc^{3+} site is very small for Eu^{2+}, and the Eu^{2+} ion can penetrate more easily into the Na^+ site than into the Sc^{3+} site. So, the solution formula can be written as $(Na_{0.980(3)}Eu_{0.020(3)})ScSi_2O_6$ on the basis of the Rietveld analysis. One can see that the Eu content in this formula is lower than that in the title formula. However, it should be kept in mind that the result was obtained without constraints. It is known that occupancies are strongly correlated with thermal parameters, and the refinement of occupancies and thermal parameters in parallel is a hard task. Moreover, it is very difficult to find the real level of small Eu content from the X-ray diffraction pattern. Therefore, the obtained result is reasonable

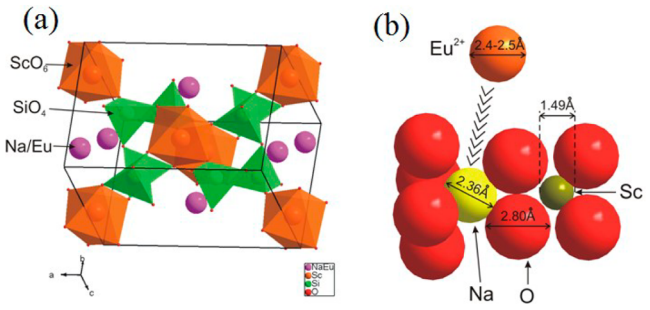

Figure 2. (a) Crystal structure of the $Na_{0.9}Eu_{0.1}ScSi_2O_6$ sample based on model (ii). (b) Schematic diagram of the structural relationship of Na^+, Sc^{3+}, and the doped Eu^{2+} in the $NaScSi_2O_6$ host.

for the Eu^{2+} site preference analysis. The Eu incorporation into the crystal lattice is additionally proofed by the cell volume increase in $Na_{0.9}Eu_{0.1}ScSi_2O_6$ up to V = 456.01(3) Å^3 in reference to the value of V = 455.2 Å^3 earlier reported for pure $NaScSi_2O_6$.[14] The volume increase can readily be related to substitution of the Na^+ ions by larger Eu^{2+} ions. Besides the Eu^{2+} site preference analysis, the Mn^{2+} site preference analysis was also conducted for the $NaScSi_2O_6$:Eu^{2+},Mn^{2+} solution. As given in the Supporting Information, the comparison of several models fitted to the Mn^{2+} sites in the $NaScSi_2O_6$ host verified that Mn^{2+} ions enter the Sc^{3+} sites. As is followed from the site occupancy observation, the $NaScSi_2O_6$:Eu^{2+} solution can be written as $Na_{1-x}ScSi_2O_6$:xEu^{2+}, and the $NaScSi_2O_6$:Eu^{2+},Mn^{2+} solution should be labeled as $Na_{1-x}Sc_{1-y}Si_2O_6$:xEu^{2+},yMn^{2+}. However, in the following part, the formulas $NaScSi_2O_6$:xEu^{2+} and $NaScSi_2O_6$:xEu^{2+},yMn^{2+} are used for clarity.

3.2. Photoluminescence Properties of the $NaScSi_2O_6$:Eu^{2+} Phosphor. The diffuse reflection spectra of undoped and Eu^{2+}-doped $NaScSi_2O_6$ are shown in Figure 3.

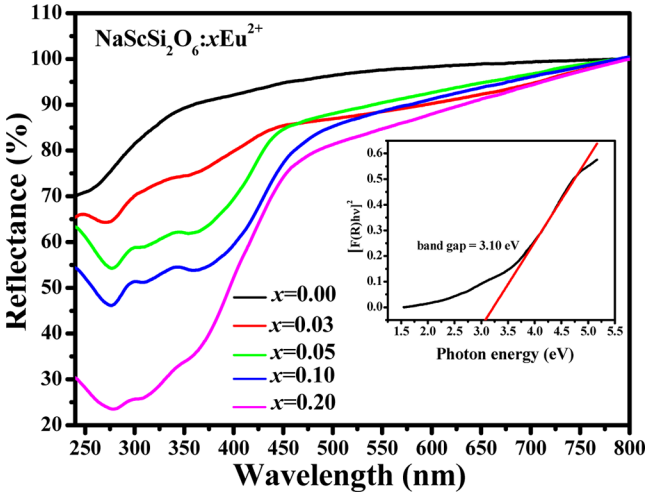

Figure 3. Diffuse reflectance spectra of $NaScSi_2O_6$:xEu^{2+} (x = 0.00, 0.03, 0.05, 0.10, and 0.20) phosphors. The inset shows the band gap calculation of the $NaScSi_2O_6$ host.

The $NaScSi_2O_6$ host material showed optical absorption over the ≤350 nm spectral region, and the band gap estimation in the $NaScSi_2O_6$ host is shown by the inset in Figure 3. The band gap of the $NaScSi_2O_6$ host can be estimated according to eq 1[24,25]

$$[F(R_\infty)h\nu]^n = A(h\nu - E_g) \quad (1)$$

dx.doi.org/10.1021/jp4062225 | J. Phys. C 2013, 117, 20847−20854

where $h\nu$ is the photon energy; A is a proportional constant; E_g is the value of the band gap; $n = 2$ for a direct transition or $1/2$ for an indirect transition; and $F(R_\infty)$ is a Kubelka–Munk function defined as

$$F(R_\infty) = (1 - R)^2/2R = K/S \quad (2)$$

where R, K, and S are the reflection, absorption, and scattering coefficient, respectively. From the linear extrapolation of $[F(R_\infty)h\nu]^2 = 0$ in the inset of Figure 3, the E_g value was estimated to be about 3.10 eV. As Eu^{2+} ions were doped into the $NaScSi_2O_6$ host, the reflection spectra of the $NaScSi_2O_6$:xEu^{2+} samples showed a strong broad absorption band over the 240–450 nm UV and n-UV range, which is attributed to the 4f–5d absorption of the Eu^{2+} ions.[26,27] The absorption edge gradually shifts to longer wavelengths, and the absorption intensity is enhanced at higher Eu^{2+} ion concentrations. The broad absorption range from 240 to 450 nm in the $NaScSi_2O_6$:xEu^{2+} phosphor matched well with the excitation spectra, which will be also discussed below.

The PLE (λ_{em} = 533 nm) spectrum of the selected $NaScSi_2O_6$:0.05Eu^{2+} and PL (λ_{ex} = 365 nm) spectra of $NaScSi_2O_6$:xEu^{2+} phosphors (x = 0.01, 0.03, 0.05, 0.10, 0.15, 0.20) are shown in Figure 4. When monitored by the emission

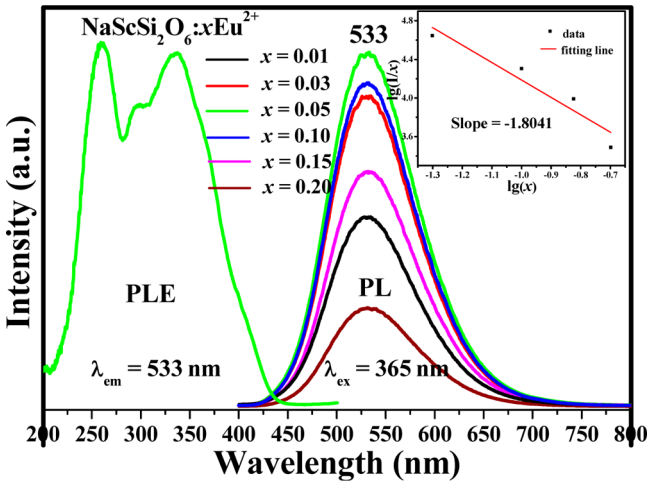

Figure 4. PLE (λ_{em} = 533 nm) and PL (λ_{ex} = 365 nm) spectra of $NaScSi_2O_6$:xEu^{2+} phosphors (x = 0.01, 0.03, 0.05, 0.10, 0.15, 0.20), and the inset shows the fitting of $\lg(I/x)$ vs $\lg(x)$ in $NaScSi_2O_6$:xEu^{2+} phosphors.

at 533 nm, the PLE spectrum exhibits a broad band in the range from 220 to 450 nm corresponding to the former diffuse reflection spectra, which is also assigned to the transitions between the ground state $4f^7$ and the crystal-field splitted $4f^65d$ configuration.[28–30] Under the excitation at 365 nm, which represented the typical emission peak available in commercial LED chips, all the PL spectra presented a broad band from 400 to 700 nm with the emission peak at around 533 nm ascribed to the electric dipole allowed transition of the Eu^{2+} ions. To understand further the origin of the observed emission center (533 nm) in the $NaScSi_2O_6$ host, the well-known empirical Van Uitert equation was considered to analyze qualitatively the experimental results. For Eu^{2+} in suitable matrices, the following eq 3 provides a good fit to the emission peak and excitation edge data. Accordingly, the emission of Eu^{2+} in $NaScSi_2O_6$ can be considered using the relation[31]

$$E = Q\left[1 - \left(\frac{V}{4}\right)^{1/V} 10^{-nrea/80}\right] \quad (3)$$

where E represents the energy position of the d-band edge for rare earth ions (cm^{-1}); Q is the energy position of the lower d-band edge for the free ions (34 000 cm^{-1} for Eu^{2+}); V is the valence of the activator (Eu^{2+}) ion ($V = 2$); n is the number of anions in the immediate shell around the Eu^{2+} ion; r is the effective radius of the host cation replaced by the Eu^{2+} ion (in Å); and "ea" is the electron affinity of the anion atoms (in eV) dependent on the anion complex type. Here, ea is approximately determined as 1.60 for the oxide host.[31] As discussed above, the Eu^{2+} ions will occupy Na^+ sites in the $NaScSi_2O_6$ host, and the calculated energy position of the d-band edge of Eu^{2+} in six-coordinated Na^+ sites (IR of $Na^+_{CN=8}$ = 1.18 Å) is 18 435 cm^{-1}, which corresponds to the Eu^{2+} emission wavelength (542 nm). It is found that the calculated value is similar to the observed Eu^{2+} emission maximum at 533 nm, and this further verified that Eu^{2+} ions are incorporated in Na^+ sites.

It is evident from Figure 4 that the emission intensity of the $NaScSi_2O_6$:xEu^{2+} phosphors increased initially with increasing Eu^{2+} concentration, reached the maximum at the Eu^{2+} concentration of ~0.05, and then decreased due to the concentration quenching effect. It is well-known that the interaction type between sensitizers or between sensitizer and activator can be calculated by the following eq 4[32,33]

$$I/x = k[1 + \beta(x)^{\theta/3}]^{-1} \quad (4)$$

where x is the activator concentration; I/x is the emission intensity (I) per activator concentration (x); k and β are constants for the same excitation condition; and θ is a function of multipole–multipole interaction. When the value of θ is 6, 8, or 10, it is the cause to say that the interaction form corresponds to dipole–dipole (d–d), dipole–quadrupole (d–q), or quadrupole–quadrupole (q–q), respectively. To get a correct θ value, the relationship between the $\lg(I/x)$ and $\lg(x)$ is plotted in the inset of Figure 4. The slope of the straight line is $-\theta/3 = -1.8041$. So, the value of θ is 5.4123, which is close to 6, meaning that the quenching results from dipole–dipole interactions in the $NaScSi_2O_6$:xEu^{2+} phosphors.

The fluorescence decay curves of Eu^{2+} emission in the $NaScSi_2O_6$:xEu^{2+} phosphors under excitation at 370 nm and monitored at 533 nm are depicted in Figure 5. The decay curves can be fitted well with the first-order exponential decay mode by eq 5[34–36]

$$I(t) = I_0 + A\exp(-t/\tau) \quad (5)$$

where I and I_0 are the luminescence intensity at time t and 0; A is a constant; t is the time; and τ is the decay time for an exponential component. On the basis of eq 5 and the measured decay curves, the lifetime values were determined to be 439.77, 409.93, 407.73, and 392.76 ns, respectively, for $NaScSi_2O_6$:xEu^{2+} phosphors with different Eu^{2+}-doped concentrations. The observed first-order exponential decay mode verified the single type of Eu^{2+} emission centers in Na^+ sites with similar chemical environment of Eu^{2+} in the $NaScSi_2O_6$ host. Furthermore, the lifetime values decrease gradually with the increasing Eu^{2+} concentration, which should be ascribed to the increase of the nonradiative and self-absorption rate of the internal doped ions when activators cross the critical separation between donor and acceptor.[37,38]

dx.doi.org/10.1021/jp4062225 | J. Phys. Chem. C 2013, 117, 20847–20854

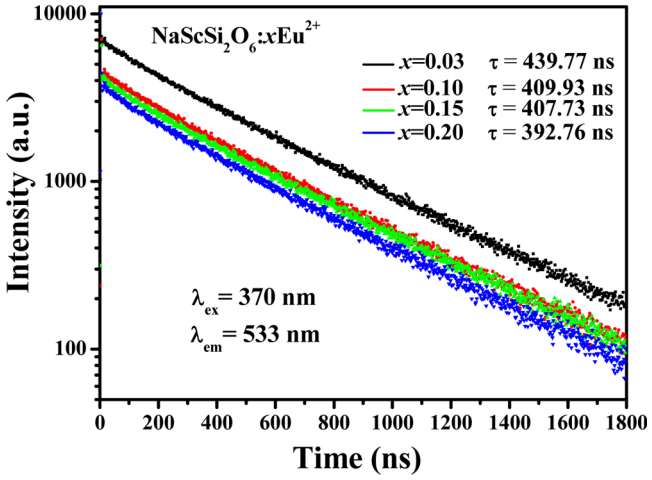

Figure 5. Decay curves of Eu^{2+} emission for $NaScSi_2O_6$:xEu^{2+} phosphors under excitation at 370 nm, monitored at 533 nm.

3.3. Generation of Red Emission by Codoping Mn^{2+} and Energy Transfer Behavior of $NaScSi_2O_6$:Eu^{2+},Mn^{2+} Phosphor. One can see that the $NaScSi_2O_6$:Eu^{2+} phosphors possess greenish yellow luminescence upon violet excitation at 365 nm. Thus, the red-emitting Mn^{2+} ions were codoped into the $NaScSi_2O_6$:Eu^{2+} phosphors to compensate the deficiency of red component due to a possible energy transfer process between Eu^{2+} and Mn^{2+}. The comparative PLE and PL spectra of $NaScSi_2O_6$:0.05Eu^{2+}, $NaScSi_2O_6$:0.10Mn^{2+}, and $NaScSi_2O_6$:0.05Eu^{2+},0.10Mn^{2+} phosphors are shown in Figure 6.

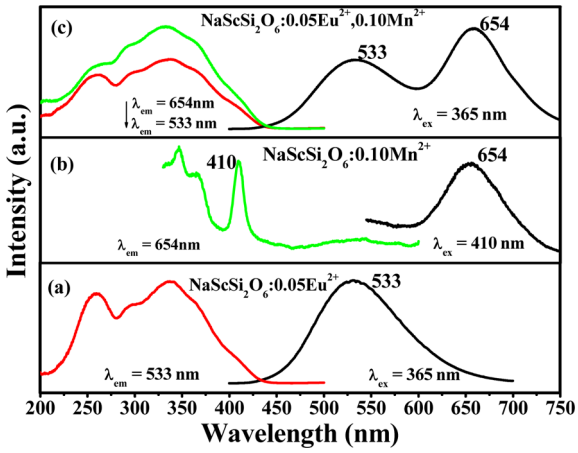

Figure 6. PLE and PL spectra of $NaScSi_2O_6$:0.05Eu^{2+}, $NaScSi_2O_6$:0.10Mn^{2+}, and $NaScSi_2O_6$:0.05Eu^{2+},0.10Mn^{2+} phosphors.

As for the PLE and PL spectra of $NaScSi_2O_6$:0.05Eu^{2+} phosphor shown in Figure 6a, they are consistent with the above analysis (Figure 4). The PLE and PL spectra of $NaScSi_2O_6$:0.10Mn^{2+} are depicted in Figure 6b. The PLE spectrum shows several distinct peaks centered at 362, 410, and 536 nm that are in good agreement with the transitions of the Mn^{2+} ions from the ground level $^6A_1(^6S)$ to $^4T_2$ (^4D), [$^4A_1$ (^4G), ^4E (^4G)], and $^4T_1$ (^4G) excited levels, respectively.[39,40] The PL spectrum represents a broad red emission band centered at 654 nm attributed to the spin-forbidden $^4T_1(^4G)-^6A_1(^6S)$ transition of the Mn^{2+} ions. A significant spectral overlap between the emission band of $NaScSi_2O_6$:0.05Eu^{2+} and the excitation band of $NaScSi_2O_6$:0.10Mn^{2+} can be seen from Figure 6a and 6b. Therefore, the energy transfer from Eu^{2+} to Mn^{2+} ions is expected in the Eu^{2+} and Mn^{2+} codoped $NaScSi_2O_6$ phosphor. As shown in Figure 6c, it gives the PLE and PL spectra of $NaScSi_2O_6$:0.05Eu^{2+},0.10Mn^{2+} phosphor, and the PLE spectrum monitored at the emission peak (654 nm) of the Mn^{2+} ions is consistent with that monitored at the emission peak (533 nm) of the Eu^{2+} ions. As a result, the excitation into the PLE band of the Eu^{2+} ions yields both the yellow emission of the Eu^{2+} and the reddish-orange emission of the Mn^{2+} ions, and the dual-color (greenish yellow/red) emission phosphor can be expected in the $NaScSi_2O_6$:Eu^{2+},Mn^{2+} phosphors with some designed compositions.

The PL spectra of $NaScSi_2O_6$:0.05Eu^{2+},xMn^{2+} phosphors, dependent on Mn^{2+} doping content (x), under excitation at 365 nm are depicted in Figure 7. With the increasing Mn^{2+}

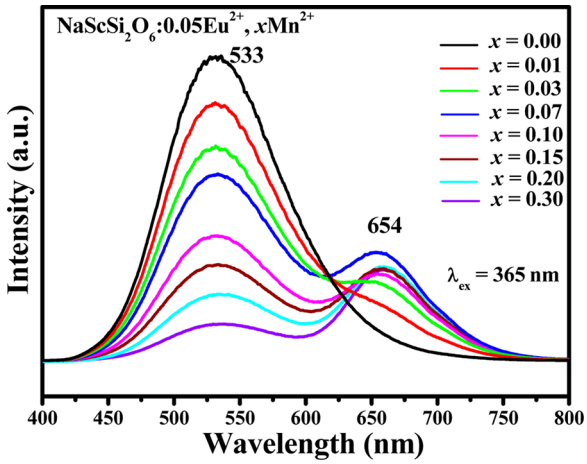

Figure 7. PL spectra of $NaScSi_2O_6$:0.05Eu^{2+},xMn^{2+} phosphors as a function of Mn^{2+} doping content (x).

concentration, one can see that the relative emission intensities of Eu^{2+} ions decrease systematically due to the energy transfer from Eu^{2+} to Mn^{2+} in the $NaScSi_2O_6$ host. Whereas the emission intensity of the Mn^{2+} ions increases with the increase of Mn^{2+} content until the maximum is reached at $x \sim 0.07$, and then the emission intensity decreases. To observe directly the relative emission intensity variation, the intensities of Eu^{2+} and Mn^{2+} emissions are given in Figure 8 as a function of the Mn^{2+} content. The observed variations in the Eu^{2+} and Mn^{2+} emission curves further support the occurrence of effective energy transfer from the Eu^{2+} to Mn^{2+} ions. Therefore, the Eu^{2+} to Mn^{2+} energy transfer efficiency (η_T) in the $NaScSi_2O_6$ host can be calculated by eq 6[41]

$$\eta_T = 1 - \frac{I_S}{I_{S0}} \quad (6)$$

where I_{S0} is the intensity of the sensitizer (Eu^{2+}) in the absence of the activator Mn^{2+} and I_S is the intensity of the sensitizer in the presence of the activator. The dependence of η_T on the Mn^{2+} doping concentration is shown in Figure 8. It is clearly observed that the value of η_T gradually increases with increasing Mn^{2+} concentration. The maximum η_T value is determined to be as high as 85.8% for the $NaScSi_2O_6$:0.05Eu^{2+},0.30Mn^{2+} phosphor.

Generally, the energy transfer from a sensitizer to an activator in a phosphor system may take place via exchange interaction and electric multipolar interaction. According to

dx.doi.org/10.1021/jp4062225 | J. Phys. Chem. C 2013, 117, 20847−20854

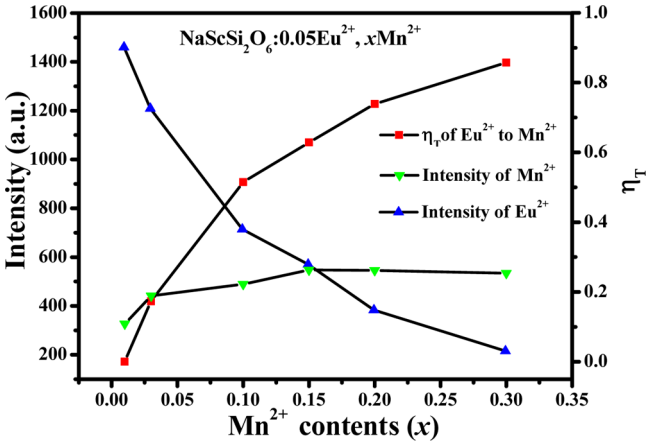

Figure 8. Dependence of the intensities of Eu^{2+} emission, Mn^{2+} emission, and the energy transfer efficiency η_T on the Mn^{2+} contents (x) for $NaScSi_2O_6$:0.05Eu^{2+},xMn^{2+} phosphors.

Dexter's energy transfer formula for the exchange and multipolar interactions, the following equation can be used to analyze the potential mechanism[42,43]

$$\eta_{so}/\eta_s \infty C^{n/3} \quad (7)$$

in which η_{so} is the intrinsic luminescence quantum efficiency of the Eu^{2+} ions; η_s is the luminescence quantum efficiency of the Eu^{2+} ions with the existence of activator (Mn^{2+}); and C is the dopant concentration of Mn^{2+}. The values of η_{so}/η_s can be approximately calculated by the ratio of related luminescence intensities (I_{so}/I_s). When the value of n is 6, 8, or 10, the form of the interaction corresponds to dipole−dipole (d−d), dipole−quadrupole (d−q), or quadrupole−quadrupole (q−q), respectively.[42,43] The I_{so}/I_s plots are illustrated in Figure 9 for

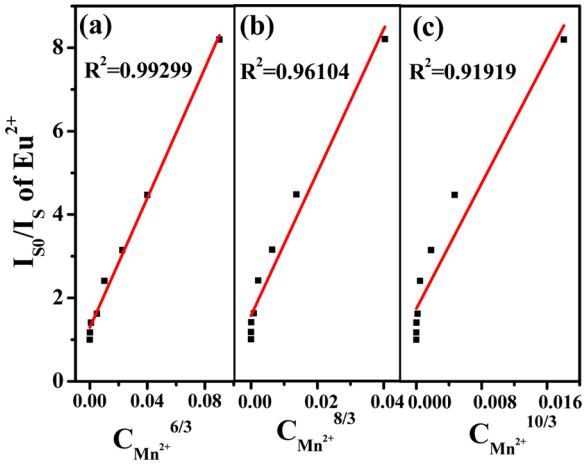

Figure 9. Dependence of I_{so}/I_s of Eu^{2+} on (a) $C_{Mn}{}^{2+6/3}$, (b) $C_{Mn}{}^{2+8/3}$, and (c) $C_{Mn}{}^{2+10/3}$ in the $NaScSi_2O_6$:0.05Eu^{2+},xMn^{2+} phosphors.

$NaScSi_2O_6$:0.05Eu^{2+},xMn^{2+} phosphors, and the relationships are tested when n = 6, 8, and 10. The linear behavior was observed only when n = 6, implying that energy transfer from Eu^{2+} to Mn^{2+} occurs via a dipole−dipole (d−d) mechanism.

3.4. CIE Values, Quantum Efficiencies, and the Application in the *w*-LED Lamp of the $NaScSi_2O_6$:Eu^{2+},Mn^{2+} Phosphor. One of the main purposes of this work is to explore the application potential of the studied phosphors. Therefore, we have studied the CIE values and quantum efficiencies of the suite of $NaScSi_2O_6$:Eu^{2+},Mn^{2+} phosphors. The CIE chromaticity coordinates for the $NaScSi_2O_6$:0.05Eu^{2+},xMn^{2+} phosphors excited at 365 nm were calculated, and a series of digital photographs of the corresponding samples under the 365 nm UV lamp are represented in Figure 10 along with the chromaticity

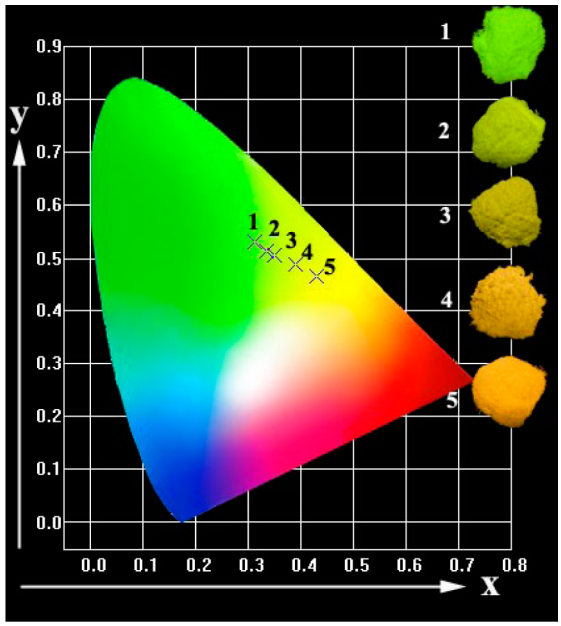

Figure 10. CIE chromaticity diagram and a series of digital photographs of the selected $NaScSi_2O_6$:0.05Eu^{2+},xMn^{2+} phosphors under 365 nm UV-lamp excitation.

coordinates in the CIE diagram. It can be obviously seen that the color tone of the phosphors shifts gradually from yellow to reddish-orange with the introduction of Mn^{2+} and the Mn^{2+} concentration increase. The corresponding chromaticity coordinates are listed in Table 2. Furthermore, the internal

Table 2. CIE Chromaticity Coordinates and Quantum Efficiencies of $NaScSi_2O_6$:0.05Eu^{2+},xMn^{2+} Samples Excited at 365 nm

samples	x (Mn^{2+})	(x, y)	IQE (%)
1	0	(0.313, 0.529)	71.7
2	0.03	(0.334, 0.512)	42.7
3	0.10	(0.350, 0.505)	40.0
4	0.15	(0.390, 0.488)	39.9
5	0.20	(0.431, 0.465)	33.0

quantum efficiencies (IQEs) of this series of $NaScSi_2O_6$:0.05Eu^{2+},xMn^{2+} phosphors measured under 364 nm excitation at room temperature are also listed in Table 2. It is found that the developed yellow-emitting $NaScSi_2O_6$:Eu^{2+} phosphor with the optimum composition possesses as high IQE as 71.7% (λ_{ex} = 365 nm), which is a little lower than that of the reported commercial yellow-emitting phosphor $Y_3Al_5O_{12}$:Ce^{3+} (86.1%) under the same experimental conditions. However, the QE can be further improved through optimization of the processing conditions and composition. Furthermore, the IQE values decrease obviously with the introduction of Mn^{2+} ions for the $NaScSi_2O_6$:0.05Eu^{2+},xMn^{2+} phosphors, which should be in relation with the energy loss in

dx.doi.org/10.1021/jp4062225 | J. Phys. Chem. C 2013, 117, 20847−20854

the Eu^{2+}−Mn^{2+} energy transfer process. Even so, such a relatively high IQE value (33.0−42.7%) is also interesting and can be concerned in the potential applications.

Accordingly, to evaluate the promise of yellow-red-emitting $NaScSi_2O_6$:0.05Eu^{2+},0.10Mn^{2+} phosphor, we combined this phosphor with commercial blue-emitting $BaMgAl_{10}O_{17}$:Eu^{2+} (BAM) to realize the white light by using *n*-UV LED chips (λ_{ex} = 370 nm). Figure 11 shows the electroluminescent (EL)

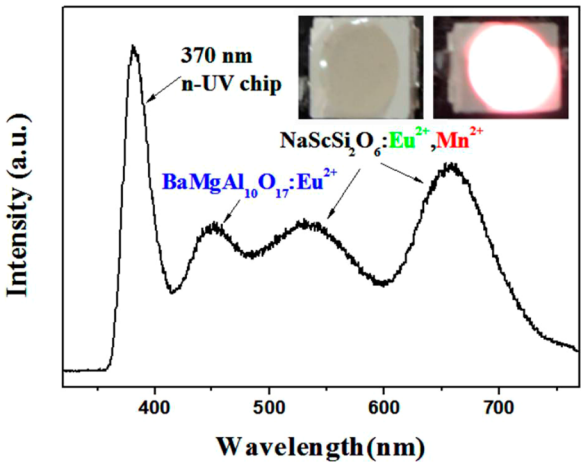

Figure 11. EL spectrum of the *w*-LED lamp based on the $NaScSi_2O_6$:0.05Eu^{2+},0.10Mn^{2+} and commercial blue BAM phosphors and driven by a current of 25 mA. The inset photographs are the *w*-LED lamp package.

spectrum of the fabricated *w*-LED lamp under 25 mA forward bias current, and the inset shows the photographs of the fabricated *w*-LED lamp and its practical emission under the same forward bias. The blue emission band (454 nm) ascribed to BAM blue phosphor and the greenish yellow and red emission bands corresponding to $NaScSi_2O_6$:0.05Eu^{2+},0.10Mn^{2+} phosphor can be observed in Figure 11; the full-color white light emission is verified. It is further found that the CIE color coordinate is (0.358, 0.378) with the warm white light emission correlated color temperature (CCT) of 4666 K and good CRI value (R_a) determined as 92.2. As discussed, $NaScSi_2O_6$:Eu^{2+} and $NaScSi_2O_6$:Eu^{2+},Mn^{2+} phosphors are promising for application in *w*-LEDs.

4. CONCLUSION

In this study, the series of greenish yellow-orange emission $NaScSi_2O_6$:Eu^{2+} and $NaScSi_2O_6$:Eu^{2+},Mn^{2+} phosphors under *n*-UV excitation is investigated for a possible application in *w*-LEDs. The structural properties of the $NaScSi_2O_6$ clinopyroxene host are evaluated, and the preferred crystallographic positions of Eu^{2+} ions are determined on the basis of Rietveld analysis and the discussion of the structure−property relationship. The photoluminescence properties of $NaScSi_2O_6$:Eu^{2+} phosphor and the energy transfer mechanism between Eu^{2+} and Mn^{2+} ions in the $NaScSi_2O_6$ lattice have also been determined. The *w*-LED lamp fabricated with $NaScSi_2O_6$:0.05Eu^{2+},0.10Mn^{2+} and commercial blue phosphors demonstrates the CIE color coordinate of (0.358, 0.378), CCT of 4666 K, and R_a value of 92.2. Thus, we believe that $NaScSi_2O_6$:Eu^{2+} and $NaScSi_2O_6$:Eu^{2+},Mn^{2+} phosphors show great potential for UV-LEDs application.

■ ASSOCIATED CONTENT

Supporting Information

CIF file of the $Na_{0.9}Eu_{0.1}ScSi_2O_6$ phase, Table S1, Table S2, and Mn^{2+} sites preference analysis for the $NaScSi_2O_6$:Eu^{2+},Mn^{2+} phosphor. This material is available free of charge via the Internet at http://pubs.acs.org.

■ AUTHOR INFORMATION

Corresponding Author

*E-mail: xiazg@cugb.edu.cn.

Notes

The authors declare no competing financial interest.

■ ACKNOWLEDGMENTS

This present work was supported by the National Natural Science Foundations of China (Grant No.51002146 and No.51272242), Natural Science Foundations of Beijing (2132050), the Program for New Century Excellent Talents in University of Ministry of Education of China (NCET-12-0950), and the Fundamental Research Funds for the Central Universities (2011YYL131). This study was also partially supported by SB RAS, Grant 28.13. Zhiguo Xia was supported by Beijing Nova Program (xx2013047). Dr. Zhiguo Xia thanks Dr. Zhiyong Mao (Shanghai Institute of Ceramics, Chinese Academy of Sciences) for the help in the fabrication of *w*-LEDs lamps.

■ REFERENCES

(1) Ye, S.; Xiao, F.; Pan, Y. X.; Ma, Y. Y.; Zhang, Q. Y. Phosphors in Phosphor-Converted White Light-Emitting Diodes: Recent Advances in Materials, Techniques and Properties. *Mater. Sci. Eng. R* **2010**, *71*, 1−34.

(2) Lin, C. C.; Liu, R. S. Advances in Phosphors for Light-Emitting Diodes. *J. Phys. Chem. Lett.* **2011**, *11*, 1268−1277.

(3) Chen, Y.; Gong, M.; Wang, G.; Su, Q. High Efficient and Low Color-Temperature White Light-Emitting Diodes with $Tb_3Al_5O_{12}$:Ce^{3+} Phosphor. *Appl. Phys. Lett.* **2007**, *91*, 071117−071117−3.

(4) Setlur, A. A.; Heward, W. J.; Gao, Y.; Srivastava, A. M.; Chandran, R. G.; Shankar, M. V. Crystal Chemistry and Luminescence of Ce^{3+}-Doped $Lu_2CaMg_2(Si,Ge)_3O_{12}$ and Its Use in LED Based Lighting. *Chem. Mater.* **2006**, *18*, 3314−3322.

(5) Xie, R. J.; Hirosaki, N.; Suehiro, T.; Xu, F. F.; Mitomo, M. A Simple, Efficient Synthetic Route to $Sr_2Si_5N_8$:Eu^{2+}-Based Red Phosphors for White Light-Emitting Diodes. *Chem. Mater.* **2006**, *18*, 5578−5583.

(6) Huang, C. H.; Chen, T. M. Novel Yellow-Emitting $Sr_8MgLn(PO_4)_7$:Eu^{2+} (Ln = Y, La) Phosphors for Applications in White LEDs with Excellent Color Rendering Index. *Inorg. Chem.* **2011**, *50*, 5725−5730.

(7) Liu, Y. F.; Zhang, X.; Hao, Z. D.; Wang, X. J.; Zhang, J. H. Tunable Full-Color-Emitting $Ca_3Sc_2Si_3O_{12}$:Ce^{3+},Mn^{2+} Phosphor via Charge Compensation and Energy Transfer. *Chem. Commun.* **2011**, *47*, 10677−10679.

(8) Lu, W.; Guo, N.; Jia, Y. C.; Zhao, Q.; Lv, W. Z.; Jiao, M. M.; Shao, B. Q.; You, H. P. Tunable Color of Ce^{3+}/Tb^{3+}/Mn^{2+}-Coactivated $CaScAlSiO_6$ via Energy Transfer: A Single-Component Red/White-Emitting Phosphor. *Inorg. Chem.* **2013**, *52*, 3007−3012.

(9) Huang, C. H.; Chiu, Y. C.; Yeh, Y. T.; Chan, T. S.; Chen, T. M. Eu^{2+}-Activated $Sr_8ZnSc(PO_4)_7$: A Novel Near-Ultraviolet Converting Yellow-Emitting Phosphor for White Light-Emitting Diodes. *ACS Appl. Mater. Interfaces* **2012**, *4*, 6661−6668.

(10) Xia, Z. G.; Zhuang, J. Q.; Liao, L. B.; Liu, H. K.; Luo, Y.; Du, P. Synthesis and Luminescence Properties of $Ba_2Gd(BO_3)_2Cl$:Eu^{2+} Phosphor. *J. Electrochem. Soc.* **2011**, *158*, J359−J362.

(11) Wu, Y. C.; Chen, T. M.; Chiu, C. H.; Mo, C. N. Luminescence and Spectroscopic Properties of Yellow-Emitting Carbonitride Phosphors and Their Application in White LEDs. *J. Electrochem. Soc.* **2010**, *157*, J342−J346.
(12) Han, J. Y.; Im, W. B.; Lee, G. Y.; Jeon, D. Y. Near UV-Pumped Yellow-Emitting Eu^{2+}-Doped $Na_3K(Si_{1-x}Al_x)_8O_{16\pm\delta}$ Phosphor for White-Emitting LEDs. *J. Mater. Chem.* **2012**, *22*, 8793−8798.
(13) Hawthorne, F. C.; Grundy, H. D. Refinement of the Crystal Structure of $NaScSi_2O_6$. *Acta Crystallogr.* **1973**, *B29*, 2615−2626.
(14) Ohashi, H.; Osawa, T.; Sato, A. $NaScSi_2O_6$. *Acta Crystallogr. C* **1994**, *50*, 838−840.
(15) Meijerink, A.; Blasse, G. Luminescence and Temperature Dependent Decay Behaviour of Divalent Europium in $Ba_5SiO_4X_6$ (X = Cl, Br). *J. Lumin.* **1990**, *47*, 1−5.
(16) Xia, Z. G.; Wang, X. M.; Wang, Y. X.; Liao, L. B.; Jing, X. P. Synthesis, Structure, and Thermally Stable Luminescence of Eu^{2+}-Doped $Ba_2Ln(BO_3)_2Cl$ (Ln = Y, Gd and Lu) Host Compounds. *Inorg. Chem.* **2011**, *50*, 10134−10142.
(17) Lin, J.; Yu, M.; Lin, C. K.; Liu, X. M. Multiform Oxide Optical Materials via the Versatile Pechini-Type Sol-Gel Process: Synthesis and Characteristics. *J. Phys. Chem. C* **2007**, *111*, 5835−5845.
(18) Zhang, C. M.; Huang, S. S.; Yang, D. M.; Kang, X. J.; Shang, M. M.; Peng, C.; Lin, J. Tunable Luminescence in Ce^{3+}, Mn^{2+}-Codoped Calcium Fluorapatite Through Combining Emissions and Modulation of Excitation: A Novel Strategy to White Light Emission. *J. Mater. Chem.* **2010**, *20*, 6674−6680.
(19) Li, G. G.; Hou, Z. Y.; Peng, C.; Wang, W. X.; Cheng, Z. Y.; Li, C. X.; Lian, H. Z.; Lin, J. Electrospinning Derived One-Dimensional LaOCl:Ln^{3+} (Ln = Eu/Sm, Tb, Tm) Nanofibers, Nanotubes and Microbelts with Multicolor-Tunable Emission Properties. *Adv. Funct. Mater.* **2010**, *20*, 3446−3456.
(20) Li, G. G.; Geng, D. L.; Shang, M. M.; Zhang, Y.; Peng, C.; Cheng, Z. Y.; Lin, J. Color Tuning Luminescence of Ce^{3+}/Mn^{2+}/Tb^{3+}-Triactivated $Mg_2Y_8(SiO_4)_6O_2$ via Energy Transfer: Potential Single-Phase White-Light-Emitting Phosphors. *J. Phys. Chem. C* **2011**, *115*, 21882−21892.
(21) Shang, M. M.; Geng, D. L.; Zhang, Y.; Li, G. G.; Yang, D. M.; Kang, X. J.; Lin, J. Luminescence and Energy Transfer Properties of $Ca_8Gd_2(PO_4)_6O_2$:A (A = Ce^{3+}/Eu^{2+}/Tb^{3+}/Dy^{3+}/Mn^{2+}) Phosphors. *J. Mater. Chem.* **2012**, *22*, 19094−19104.
(22) *Bruker AXS TOPAS V4: General Profile and Structure Analysis Software for Powder Diffraction Data. − User's Manual*; Bruker AXS: Karlsruhe, Germany, 2008.
(23) Shannon, R. D. Revised Effective Ionic Radii and Systematic Studies of Interatomic Distances in Halides and Chalcogenides. *Acta Crystallogr. A* **1976**, *32*, 751−767.
(24) Yamashita, N. Luminescence Centers of Ca(S:Se) Phosphors Activated with Impurity Ions Having s^2 Configuration. I. Ca(S:Se):Sb^{3+} Phosphors. *J. Phys. Soc. Jpn.* **1973**, *35*, 1089.
(25) Zhou, J.; Xia, Z. G.; Yang, M. X.; Shen, K. High Efficiency Blue-Emitting Phosphor: Ce^{3+}-Doped $Ca_{5.45}Li_{3.55}(SiO_4)_3O_{0.45}F_{1.55}$ for Near UV-Pumped Light-Emitting Diodes. *J. Mater. Chem.* **2012**, *22*, 21935−21941.
(26) Blasse, G.; Grabmaier, B. C. *Luminescent Materials*; Springer Verlag: Berlin, 1994.
(27) Im, W. B.; Fellows, N. N.; DenBaars, S. P.; Seshadri, R.; Kim, Y. $LaSr_2AlO_5$, a Versatile Host Compound for Ce^{3+}-Based Yellow Phosphors: Structural Tuning of Optical Properties and Use in Solid-State White Lighting. *Chem. Mater.* **2009**, *21*, 2957−2966.
(28) Dorenbos, P. Energy of the First $4f^7 \rightarrow 4f^6 5d$ Transition of Eu^{2+} in Inorganic Compounds. *J. Lumin.* **2003**, *104*, 239−260.
(29) Xia, Z. G.; Li, Q.; Sun, J. Y. Luminescence Properties of $Ba_5SiO_4(F, Cl)_6$:Eu^{2+} Phosphor. *Mater. Lett.* **2007**, *61*, 1885−1888.
(30) Xia, Z. G.; Sun, J. Y.; Du, H. Y.; Zhou, W. Luminescence of Eu^{2+} in Alkali Earth Chlorosilicate Phosphor and Their Color-Tunable Properties. *Opt. Mater.* **2006**, *28*, 524−529.
(31) Van Uitert, L. G. An Empirical Relation Fitting the Position in Energy of the Lower d-band Edge for Eu^{2+} or Ce^{3+} in Various Compounds. *J. Lumin.* **1984**, *29*, 1−9.
(32) Ozawa, L.; Jaffe, P. M. The Mechanism of the Emission Color Shift with Activator Concentration in +3 Activated Phosphors. *J. Electrochem. Soc.* **1971**, *118*, 1678−1679.
(33) Van Uitert, L. G. Characterization of Energy Transfer Interactions between Rare Earth Ions. *J. Electrochem. Soc.* **1967**, *114*, 1048−1053.
(34) Shang, M. M.; Li, G. G.; Kang, X. J.; Yang, D. M.; Geng, D. L.; Lin, J. Tunable Luminescence and Energy Transfer Properties of Sr_3AlO_4F:RE^{3+} (RE = Tm/Tb, Eu, Ce) Phosphors. *ACS Appl. Mater. Interfaces* **2011**, *3*, 2738−2746.
(35) Hao, J.; Studenikin, S. A.; Cocivera, M. Transient Photoconductivity Properties of Tungsten Oxide Thin Films Prepared by Spray Pyrolysis. *J. Appl. Phys.* **2001**, *90*, 5064−5069.
(36) Xia, Z. G.; Zhuang, J. Q.; Meijerink, A.; Jing, X. P. Host Composition Dependent Tunable Multicolor Emission in the Single-Phase $Ba_2(Ln_{1-z}Tb_z)(BO_3)_2Cl$:Eu Phosphors. *Dalton Trans.* **2013**, *42*, 6327−6336.
(37) Li, Y. C.; Chang, Y. H.; Chang, Y. S.; Lin, Y. J.; Laing, C. H. Luminescence and Energy Transfer Properties of Gd^{3+} and Tb^{3+} in $LaAlGe_2O_7$. *J. Phys. Chem. C* **2007**, *111*, 10682−10688.
(38) Xia, Z. G.; Liu, R. S.; Huang, K. W.; Drozd, V. $Ca_2Al_3O_6F$:Eu^{2+}: A Green-Emitting Oxyfluoride Phosphor for White Light-Emitting Diodes. *J. Mater. Chem.* **2012**, *22*, 15183−15189.
(39) Guo, N.; Jia, Y. C.; Lü, W.; Lv, W. Z.; Zhao, Q.; Jiao, M. M.; Shao, B. Q.; You, H. P. A Direct Warm-White-Emitting $Sr_3Sc(PO_4)_3$:Eu^{2+},Mn^{2+} Phosphor with Tunable Photoluminescence via Efficient Energy Transfer. *Dalton Trans.* **2013**, *28*, 5649−5654.
(40) Wu, W.; Xia, Z. G. Synthesis and Color-Tunable Luminescence Properties of Eu^{2+} and Mn^{2+}-Activated $Ca_3Mg_3(PO_4)_4$ Phosphor for Solid State Lighting. *RSC Adv.* **2013**, *3*, 6051−6057.
(41) Paulose, P. I.; Jose, G.; Thomas, V.; Unnikrishnan, N. V.; Warrier, M. K. R. Sensitized Fluorescence of Ce^{3+}/Mn^{2+} System in Phosphate Glass. *J. Phys. Chem. Solids* **2003**, *64*, 841−846.
(42) Dexter, D. L. A Theory of Sensitized Luminescence in Solids. *J. Chem. Phys.* **1953**, *21*, 836−850.
(43) Blasse, G. Energy Transfer in Oxidic Phosphors. *Philips Res. Rep.* **1969**, *24*, 131−144.